Superlattice magnetophonon resonances in strongly coupled InAs/GaSb superlattices

R. S. Deacon, R. J. Nicholas,* and P. A. Shields
Clarendon Laboratory, University of Oxford, Parks Road, Oxford OX1 3PU, United Kingdom

A. B. Henriques
Instituto de Fisica, Universidade de São Paulo, Caixa Postal 66318, 05315-970 São Paulo, Brazil
(Received 9 January 2007; revised manuscript received 16 May 2007; published 8 August 2007)

We report an experimental study of miniband magnetoconduction in semiconducting InAs/GaSb superlattices. For samples with miniband widths below the longitudinal optical phonon energy we identify a superlattice magnetophonon resonance caused by resonant scattering of electrons across the mini-Brillouin zone. This resonant feature arises directly from the superlattice dispersion and total magnetic quantization (energetic decoupling) of the superlattice Landau level minibands.

DOI: 10.1103/PhysRevB.76.075309 PACS number(s): 73.21.Cd, 73.43.Qt

I. INTRODUCTION

Semiconductor superlattices (SL's) comprise alternating layers of two or more semiconductor materials, leading to the formation of continuous energy bands in the growth direction, called minibands. The reduced Brillouin zone and energy bandwidth of the SL allow measurements that probe parameter spaces that are inaccessible in bulk semiconductors. Total quantization of the superlattice energy scheme can be achieved by the application of a large magnetic field, which suppresses inter-Landau-level miniband (LLMB) scattering and allows the realization of a "quasi-one dimensional" or quantum box SL (QBSL) regime. This has led to strong interest in the SL magnetoresistance and transport characteristics.[1–5] The SL miniband structure can be engineered such that in the QBSL regime optical phonon scattering is limited[6,7] by using narrow minigap and miniband widths, leaving only weak acoustic phonon processes to dissipate the electron energy. In this paper, we investigate magnetotransport properties of InAs/GaSb superlattices in the miniband transport regime. In a previous publication[5] we investigated hot-electron magnetophonon resonance caused by the LO-phonon-mediated hopping between Landau Wannier-Stark states at low temperatures. In this paper, we study longitudinal magnetophonon resonances caused by the resonant emission or absorption of longitudinal optical phonons in the miniband transport regime for a range of SL structures at high temperatures. Through a systematic study using different miniband widths we identify a form of magnetophonon resonance that provides evidence for the energetic decoupling of SL Landau level minibands, leading to suppression of optical phonon scattering.

The Bloch frequency (Ω) of a biased SL is given by $\Omega = eFd/\hbar$ where F is the applied electric field and d is the superlattice period. Superlattice transport at low temperatures is characterized by two regimes. At low electric fields where $\hbar\Omega < \Delta$, where Δ is the SL miniband width, miniband transport through extended SL states dominates. In the simple Esaki-Tsu miniband transport model,[8] electron drift velocity (v) is described by a scattered Bloch oscillator in one dimension, $v = \mu F/[1+(F/F_c)^2]$, where electron mobility $\mu = e\Delta\tau d^2/2\hbar^2$, $F_c = \hbar/e\tau d$, and τ is the scattering time. The main mechanisms that contribute to τ are phonon scattering, impact ionization, and interface roughness scattering. At high electric fields, however, $\hbar\Omega > \Delta$, causing the miniband to split into localized Wannier-Stark-ladder (WSL) states[9–11] and consequently miniband transport is no longer the dominant process.

Despite the critical role of energy relaxation processes in superlattices the magnetophonon effect[12] has only received a small amount of attention. It has been extensively studied in bulk[13–15] and two-dimensional[16] semiconductor systems, where magnetophonon resonances (MPR's) are observed as magnetoresistance oscillations caused by resonant scattering of electrons by optical phonons. The dominant electron-phonon coupling in all III-V systems is with the LO phonon due to the large electric polarization associated with these modes. Conservation of crystal momentum limits the LO phonon scattering to phonons near the Brillouin zone center such that the LO phonon energy is essentially monoenergetic.

The effects of MPR on the resistivity depend strongly on the relative configuration of the applied electric and magnetic fields. In the transverse case ($F \perp B$), resonant momentum relaxation causes magnetoresistance maxima to be observed at precisely the MPR resonance condition

$$\delta n \omega_c = \omega_{LO}, \tag{1}$$

where ω_c is the cyclotron frequency, ω_{LO} is the LO phonon frequency, and δn is an integer. At B fields that satisfy the MPR condition, strong inelastic scattering occurs between zero momentum states separated in Landau index by δn. In the longitudinal configuration ($F \| B$) considered in this paper, the MPR is typically more complicated as direct LO phonon emission and absorption processes between zero-momentum states do not relax the electron momentum in the electric field direction. In bulk materials, resonances occur due to an interplay of different indirect scattering processes.[14,17] Extensive experimental observations of longitudinal MPR (LMPR) in bulk III-V systems[13,14] reveal resistivity minima which are displaced to B fields somewhat below condition (1). Calculations for superlattices have suggested both that resistivity minima[18] should occur at fields slightly below the resonance condition and that max-

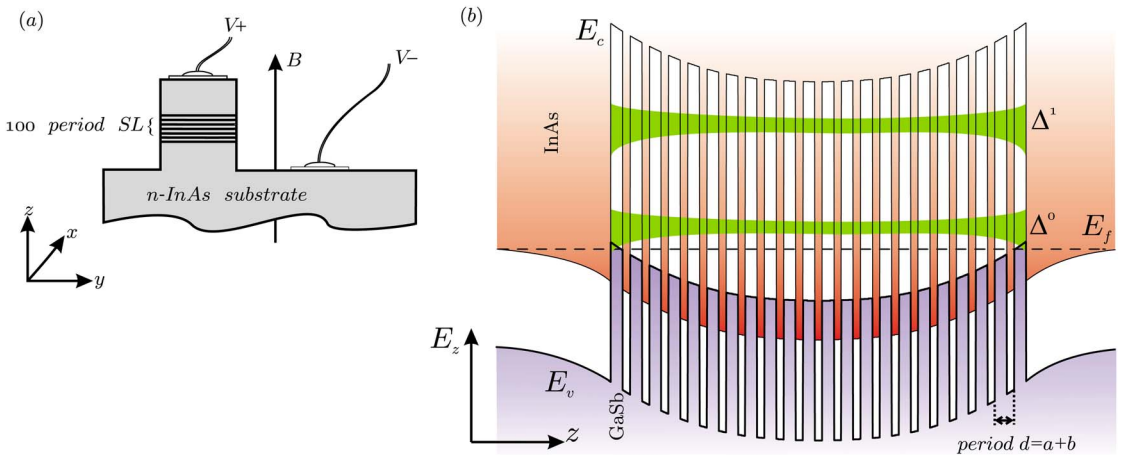

FIG. 1. (Color online) (a) Schematic of sample geometry. (b) Schematic of the sample potential profile for a 22-period SL without an applied bias displaying the effect of sample-substrate and sample-cap inversion layers, which broaden the superlattice miniband and facilitate electron injection into the structure. This schematic picture is supported by self-consistent $\mathbf{k}\cdot\mathbf{p}$ simulations.

ima could occur[19,20] at the resonance condition. When Δ is significantly below the LO phonon energy Polyanovskii[20,21] has also suggested that transitions from the top to the bottom of the miniband will generate superlattice magnetophonon resonances (SLMPR's) at the condition

$$\delta n\hbar\omega_c = \hbar\omega_{LO} + \Delta, \tag{2}$$

where resonant LO phonon scattering between areas of high density of states (DOS) at the top and bottom of the superlattice miniband enhances the current.

In contrast to the predictions of theory all experimental observations of MPR in superlattices[22–24] have assigned MPR features as resistance maxima, predominantly in samples with low Δ and using the GaAs/AlAs system. A significant enhancement of the resonant peak intensity, compared with bulk material, has been reported and attributed to the effect of the superlattice band structure. Noguchi *et al.*[22] also observed that low Δ samples exhibited plateaus in the oscillatory part of the magnetoresistance trace, which it was suggested may provide evidence for Polyanovskii's predictions. Detailed studies by Gassot *et al.*[23] also assigned LMPR peaks as maxima in resistance but reported significant deviations from the predicted MPR conditions. The analysis of the GaAs/AlAs system is further complicated by the presence of resonances attributed to both the GaAs and AlAs LO phonons, which are approximately 25% different in energy.

This paper reports studies of the magnetophonon effect in the type-II InAs/GaSb system, which has a low carrier effective mass ($m^* \sim 0.05m_e$) allowing the study of transport at cyclotron energies considerably above the LO phonon energy ($\hbar\omega_{LO}$=30 meV). The analysis of the resonance is also simplified because the LO phonon energies of the InAs and GaSb layers are almost exactly equal. Tunneling between adjacent superlattice layers is dominated by interband coupling and is strongly $\mathbf{k}$ dependent. The interband coupling to the barrier valence band states is strongly reduced for higher Landau index (n) LLMB's resulting in narrower miniband widths[25] [$\Delta_n(B)$] and suppressing domain formation.

Throughout this report we will refer to all experimentally observed resonances as LMPR features so as to distinguish them from the MPR condition. This is important as the longitudinal configuration typically produces resonances slightly shifted from the MPR condition.

II. EXPERIMENTAL METHOD

Experiments were performed on 100 period undoped InAs/GaSb superlattices grown by MOVPE. Samples were grown on n-type InAs substrates (carrier density $\sim 5 \times 10^{15}$ cm^{-3} estimated from Shubnikov–de Haas measurements) with 5000 Å InAs buffer and cap layers. The ratio of InAs/GaSb (a:b) is estimated from growth rates measured using an *in situ* surface photoabsorption (SPA) technique.[26] Samples were also characterized using x-ray diffraction (XRD), allowing calculation of the superlattice period (d=a+b).

For vertical transport measurements 150 μm mesas were defined using standard lithographic and wet etching techniques. Ohmic contacts were made to sample and substrate by evaporating 5 nm of chromium and 150 nm of gold. Pre-

TABLE I. Sample characteristics.

Sample no.	d (Å)[a]	d_{InAs}:d_{GaSb}[b]	$\Delta_{n=0}(0)$ (meV)[c]	p[d]
4577	166	0.29	2	56
4562	130	0.46	10	60
4561	126	0.50	13	59
4579	117	0.83	27	62
3756	93	0.82	48	67
4520	86	1.26	75	60

[a]Measured with XRD.
[b]Estimated with SPA data.
[c]Estimated using $\mathbf{k}\cdot\mathbf{p}$ calculations (±15% error).
[d]Estimated from Stark cyclotron resonances and hot-electron MPR; see Refs. 5 and 27.

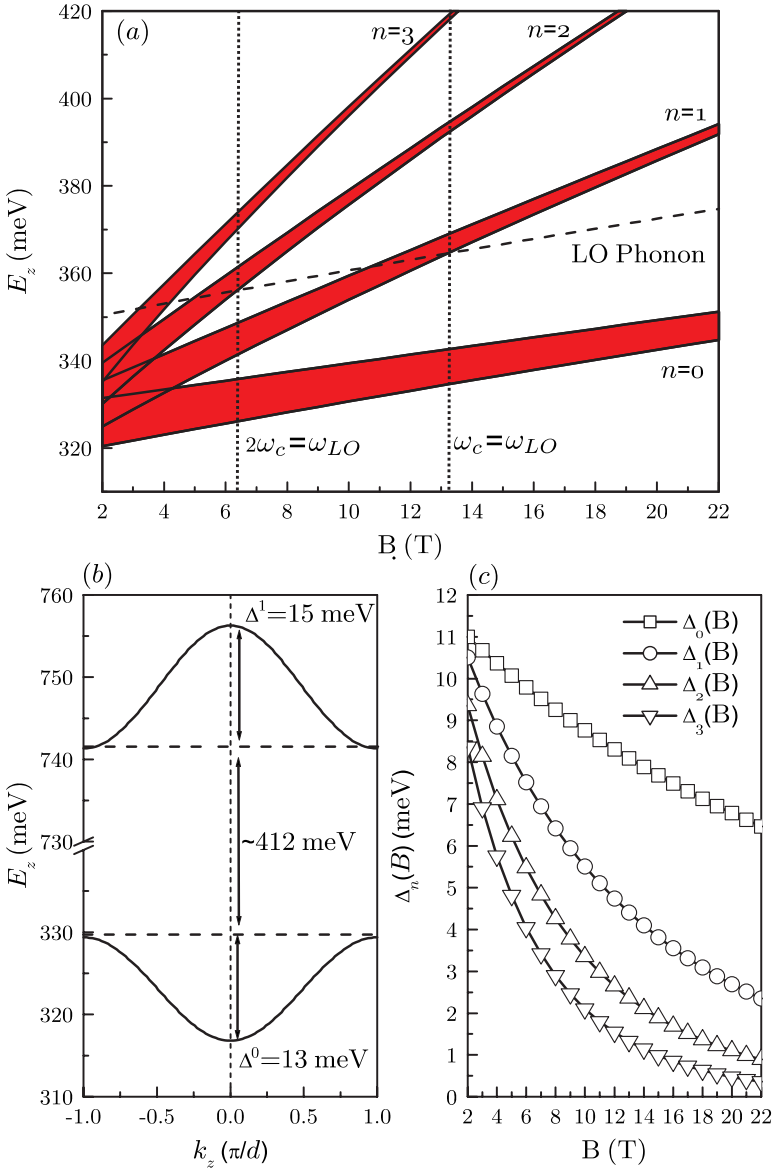

FIG. 2. (Color online) Example $\mathbf{k}\cdot\mathbf{p}$ simulation results for sample 4561. (a) Landau miniband fan calculated from average of spin-up and down levels. The dashed line marks the LO phonon energy and fundamental MPR condition. (b) Miniband dispersion for the first and second SL minibands at $B=0$ T. (c) Plot of the magnetic field dependence of the first four Landau minibands.

vious measurements[5,27] on the same samples have identified that transport is best described by a number of active periods which is less than the nominal 100 periods grown. Reduction in the number of periods is caused by the formation of InAs inversion layers at the superlattice-substrate and superlattice-cap interfaces [Fig. 1(b)]. Low-temperature measurements on these samples identify two-dimensional electron gases with carrier densities $\sim 1\times 10^{12}$ cm^{-2}, from Shubnikov–de Haas-like oscillations, which is consistent with the formation of this structure. Electron wave functions in the miniband couple with the inversion layer states causing a widening of the superlattice miniband in some of the first and last periods of the structure. The broadened miniband states are highly conducting and allow electrons to be easily injected into the miniband. The broadened miniband also exhibits negligible voltage drop when the structure is biased, resulting in the reduction of the number of active periods observed (p).

All measurements were performed in dc mode with two contacts as displayed schematically in Fig. 1(a). $R(B)$ measurements in magnetic fields up to 19.5 T were performed using a superconducting magnet system and a Keithley 236 source measure unit. Higher magnetic fields were obtained using nondestructive magnets in the Clarendon Laboratory Kurti pulsed magnetic field facility. The magnetic field pulse was recorded using a pickup coil situated 2 mm below the sample. Induced voltages during the magnetic field pulse are removed by averaging two pulses of opposite polarity. Pulsed field measurements were performed with Gage Compuscope 5 MHz transient recorder cards.

Sample characteristics were simulated with $\mathbf{k}\cdot\mathbf{p}$ theory[28] solved using the envelope function approximation[29] in momentum space.[30] Sample characteristics are summarized in Table I. Fourier transform magnetoabsorption spectroscopy was used to observe the superlattice energy gap which allows refined estimation of the ratio $a:b$ and shows that miniband width estimates in Table I are correct within to ±15%. $\mathbf{k}\cdot\mathbf{p}$ simulation of the superlattice Landau miniband fan are later used to predict the position of MPR features. An example of a SL Landau miniband fan is presented in Fig. 2 for sample 4561. All samples display a large separation between the first

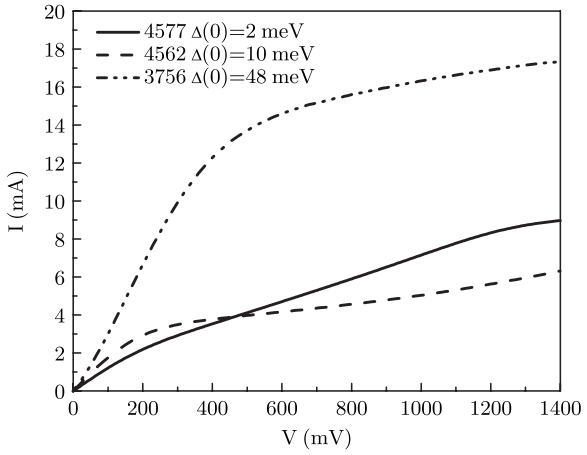

FIG. 3. $I(V)$ characteristic of samples 4577 and 4562 at $T=80$ K and 3756 at $T=77$ K.

and second conduction minibands (~400 meV for 4561) such that for the bias values used in this study only conduction through the fundamental miniband needs be considered [Fig. 2(b)]. Simulation results also clearly display a strong suppression of miniband width with increasing magnetic field, which is stronger for higher-index Landau levels due to the higher energy of these states [Fig. 2(c)].

III. RESULTS

$I(V)$ curves for three samples are displayed in Fig. 3 and are characteristic of the response of all superlattices studied in this paper. We observe conventional miniband transport characteristics with a region of Ohmic miniband transport at low bias followed by a miniband transport peak identified as a shoulder in the $I(V)$ trace (for example, at ~200 mV for sample 4577 and ~600 mV for sample 3756). For sample 4577 we observe a second shoulder at ~1250 mV that is attributed to electron-phonon resonances in the Stark hopping regime,[31,32] as discussed in a previous publication on hot-electron MPR observed in the WSL regime for the same sample set.[5]

$R(B)$ curves for sample 4577 [$\Delta_0(0)=2$ meV] are displayed in Fig. 4(a) for bias in the range 0–1000 mV and $T=80$ K. $R(B)$ traces are analyzed by plotting d^2R/dB^2 to remove the monotonically increasing background resistance and identify weak resonances [Fig. 4(b)]. In plots of d^2R/dB^2, maxima correspond to resistivity minima in the equivalent $R(B)$ trace. In this paper we will use the simplification that the additional resistivity maxima and minima caused by the resonant scattering processes refer to minima and maxima in d^2R/dB^2, respectively, a simplification in discussion often used when discussing MPR features.[33] Plots of d^2R/dB^2 display strong maxima features at $B\sim 13, 15$ T and $B\sim 6.3$, 8 T. Estimates of the $\delta n=1$ MPR condition for sample 4577 using $\mathbf{k}\cdot\mathbf{p}$ calculations predict a resonance at $B=14.2$ T.

The appearance of two resonant peaks close to the conventional magnetophonon condition predicted by $\mathbf{k}\cdot\mathbf{p}$ calculations suggests that the resonant behavior may be significantly more complex than has previously been assumed. The main resistivity maximum lies close to the conventional MPR condition [Eq. (1)], while the resistivity minimum that might be attributed to LMPR is at $B\sim 12.8$ T shifted to ~8% below the conventional MPR condition. The second minimum at $B\sim 15$ T is a possible example of the additional SLMPR resonance given by Eq. (2). This assignment is supported by the fact that both LMPR and SLMPR features are significantly suppressed with increasing bias beyond ~200 mV when the superlattice moves into the WSL regime, and so all further measurements were restricted to the miniband transport range of bias. The feature at ~8 T is likely to be the $\delta n=2$ SLMPR resonance. Assignment of the 6.3 T feature to $\delta n=2$ LMPR is, however, inconclusive as a residual Shubnikov–de Haas oscillation peak for the bulk substrate occurs at approximately 6 T and complicates analysis in this low-B-field region.

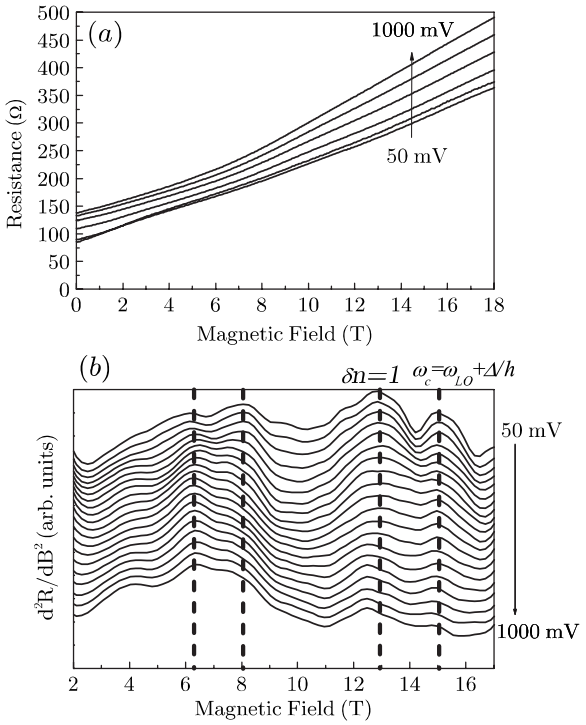

FIG. 4. (a) $R(B)$ curves for sample 4577 at $T=80$ K for a range of bias. (b) Plot of d^2R/dB^2 for sample 4577 with $T=80$ K and a range of sample bias. Vertical dashed lines mark the observed LMPR and SLMPR features.

In order to test this assignment results are examined for samples with a range of miniband widths as shown in Fig. 5. The strong features identified for analysis are selected for repeatability between successive measurements and in comparison with data taken for steady fields up to 19 T, as shown for sample 4577 in Fig. 4. Resistivity minima (d^2R/dB^2 maxima) that are candidates for LMPR and SLMPR features are indicated by arrows. As the miniband width increases, the separation of the SLMPR feature from the conventional MPR resonance increases progressively. All features show a characteristic MPR temperature dependence with maximum amplitude in the range $T=80$–140 K.

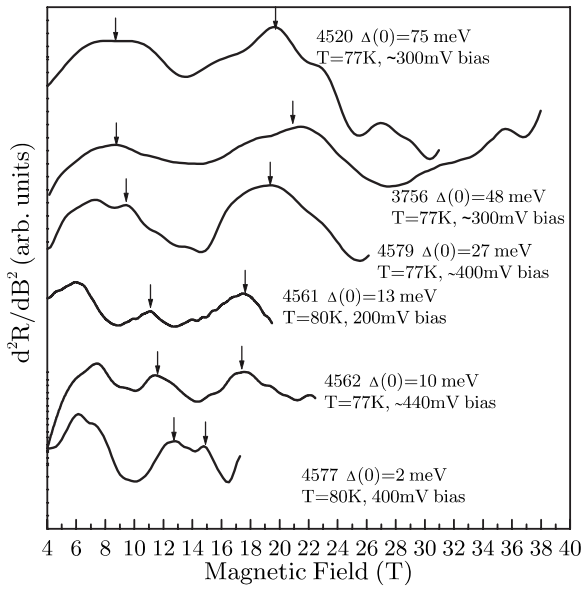

FIG. 5. Plot of d^2R/dB^2 for a range of superlattice samples.

IV. DISCUSSION

The magnetic field positions of the observed LMPR and SLMPR minima and maxima features are compared with the values predicted by $\mathbf{k}\cdot\mathbf{p}$ calculations and Eqs. (1) and (2) in Fig. 6. The $\mathbf{k}\cdot\mathbf{p}$ predicted magnetic field value for the MPR condition falls with increasing Δ due to the decrease in the superlattice band gap, which causes the effective mass to decrease. We observe that resistivity maxima (d^2R/dB^2 minima) occur at fields slightly above the conventional MPR resonance position. The experimentally observed resistivity minima labeled as $\delta n=1$ LMPR are typically seen when $\omega_c/\omega_{LO}=0.87\pm0.06$, in good agreement with bulk LMPR resonances.[13,14] By contrast, the SLMPR features move up in field due to the increased contribution from Δ in Eq. (2) and show excellent agreement with the predicted SLMPR positions when account is taken of the magnetic field dependence of the miniband width.

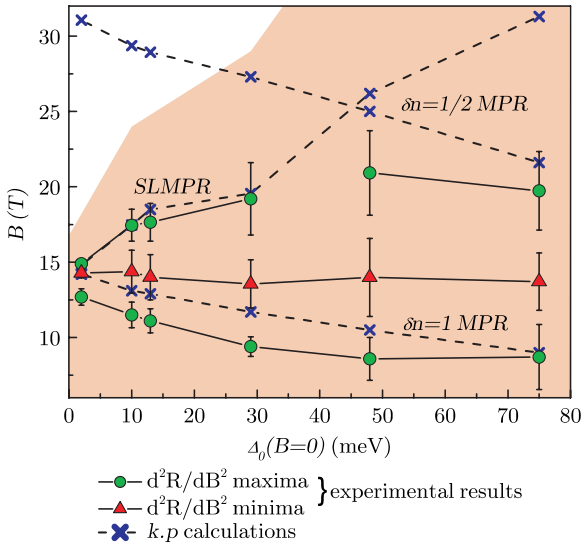

FIG. 6. (Color online) Plot of predicted LMPR and SMPR features from $\mathbf{k}\cdot\mathbf{p}$ calculations alongside experimentally observed resonances. The x axis indicates the SL miniband width at $B=0$ T calculated with $\mathbf{k}\cdot\mathbf{p}$. Note that the $\mathbf{k}\cdot\mathbf{p}$-calculated resonance positions take account of the reduction in SL miniband width with increasing magnetic field which becomes particularly significant for the three highest-miniband-width samples. As there is no predicted line shape for the resonances the errors are estimated from 40% full width half maximum of the features. Shaded region indicates the parameter space experimentally probed.

As the miniband width increases we expect a continuous transition to conventional bulk magnetophonon behavior once $\Delta_0(B)>\hbar\omega_{LO}$, since the superlattices may be considered to act as a bulk three-dimensional system if all thermal and cyclotron excitations are much smaller than the superlattice miniband width,

$$k_BT,\hbar\omega_c,\hbar\omega_{LO}\ll\Delta_0(B). \tag{3}$$

Within this regime, electrons are unable to probe the upper portion of the superlattice miniband and carriers only experience a dispersion similar to the parabolic bulk case. It would therefore be expected that such samples display no SLMPR features. $\mathbf{k}\cdot\mathbf{p}$ calculation results for samples 3756 and 4520 indicate that, if observed, the SLMPR would be located at $B=26.1$ and 31.3 T, respectively. In experiment (Fig. 5) both exhibit resistance minima features at around 20 T that correspond well with the predicted $\delta n=1/2$ MPR resonance, which is also particularly strong in the longitudinal configuration for bulk materials,[14] suggesting that the transition to bulk behavior has occurred for these structures. This will be discussed further later in this paper.

The physical origins of the LMPR and SLMPR features in low-miniband-width samples $[\Delta_0(0)<\hbar\omega_{LO}]$ can be understood by considering the LO phonon absorption and emission processes that are allowed for different ω_c values, as shown in Fig. 7. Interminiband LO phonon scattering between the $n=0$ and $n=1$ LLMB's is permitted only in the range $\omega_{LO}-\Delta_1/\hbar<\omega_c<\omega_{LO}+\Delta_0/\hbar$ due to the forbidden energy gaps in the system. Note also that the miniband width of any given LLMB has a significant magnetic field dependence $[\Delta_n(B)]$, further complicating this schematic picture. Transitions for which final or initial states are at $k_z=0$ and/or the mini-Brillouin-zone boundary $k_z=\pm\pi/d$ have high scattering rates due to the large density of states at these k_z.

We can consider the scattering of electrons in the positive k_z region of the $n=0$ LLMB dispersion which contribute to the transport current. It is clear that LO phonon absorption transitions will result in final states at $+k$ and $-k$ such that the average velocity of a final state is zero. The average of LO phonon scattering events therefore relaxes the electron momentum, and the resistance will be proportional to the scattering rate. The scattering rate will increase on approaching the MPR condition as LO phonon scattering is allowed over a greater proportion of the dispersion. At the MPR condition, the LO phonon scattering rate is at its greatest. If $\Delta_0=\Delta_1$, scattering will be allowed anywhere within the superlattice dispersion. In reality, $\Delta_0>\Delta_1$ for the InAs/GaSb system restricting scattering at the mini-Brillouin-zone boundary.

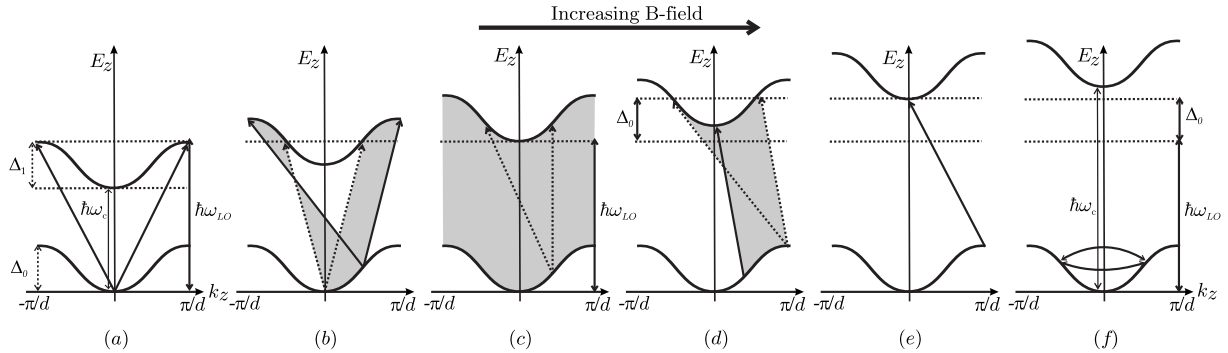

FIG. 7. Schematics of the LO-phonon-mediated transitions for narrow-miniband-width samples $[\Delta_0(0)<\hbar\omega_{LO}]$ between the $n=0$ and $n=1$ LLMB's. Transitions are highlighted at (a) $\omega_c=\omega_{LO}-\Delta_1/\hbar$, (b) $\omega_{LO}>\omega_c>\omega_{LO}-\Delta_1/\hbar$, (c) $\omega_c=\omega_{LO}$ (the MPR condition), (d) $\omega_{LO}+\Delta_0/\hbar>\omega_c>\omega_{LO}$, (e) $\omega_c=\omega_{LO}+\Delta_0/\hbar$, and (f) $\omega_c>\omega_{LO}+\Delta_0/\hbar$. The allowed LO-phonon-mediated transitions from areas of positive k_z are indicated by the shaded region.

Above the MPR condition the scattering rate is reduced with increasing B field as LO phonon transitions from the center of the superlattice dispersion are increasingly forbidden. At the SLMPR condition $(\omega_c=\omega_{LO}+\Delta_0/\hbar)$ only scattering from $k_z=\pm\pi/d$ in the $n=0$ LLMB to $k_z=0$ in the $n=1$ LLMB is allowed. The relaxation therefore links two high-density-of-states regions of the dispersion relation, resulting once again in a high scattering rate.

For superlattice miniband transport, however, the current flow is dependent on more than simply the immediate scattering rate. The contribution to current flow also depends on the subsequent ballistic motion in k space under electric field acceleration, since the velocity is strongly dependent upon where the carrier is in the dispersion relation. These factors must be considered to fully understand the form of MPR features. We consider the relative effects of acceleration of carriers in initial and final scattered states to determine the effect of the scattering upon transport current. Acceleration in an electric field following LO phonon scattering has the effect of decreasing drift velocity below the MPR condition, since the carrier velocity is increasing with k in the lower Landau level and decreasing with k in the upper level [Fig. 7(b)]. Conversely, the drift velocity increases above the MPR condition. At the MPR condition, final and initial states are comparable such that subsequent acceleration does not alter the total transport current. Scattering at the SLMPR condition has the most dramatic and significant consequence that it prevents the occurrence of Bragg scattering and the subsequent suppression of transport current due to cycling of the carriers through the negative drift velocity section of the dispersion relation. Above $\hbar\omega_c=\hbar\omega_{LO}+\Delta_0(B)$, the coupling of the $n=0$ and $n=1$ LLMBs through LO phonon scattering is removed and intra-LLMB scattering dominates. This reverses carrier momentum and quenches transport,[2,4] resulting in a significant increase in resistance following the SLMPR feature. The characteristics of the LMPR and SLMPR features are therefore determined by interplay of the scattering rate and the subsequent ballistic motion of the transport electrons. This simple analysis indicates that LMPR is likely to appear as a resistance maximum at the MPR condition due to the high scattering rate and SLMPR as a resistance minimum followed by a large increase in resistance.

In order to understand the different contributions to the magnetoresistance, modeling of the experimental results was therefore performed using semiclassical Monte Carlo simulations of the miniband transport, assuming that the effects of Wannier-Stark localization are not significant. Simulations follow the method outlined by Henriques *et al.*[4] Limited inelastic acoustic phonon scattering in an energy window of 1 meV (selected to be less than Δ) was introduced to ensure that the conductivity at high B fields is small but nonzero. It is found that changing this window significantly alters the background magnetoresistance but that the LMPR and SLMPR features remain. Simulation results are displayed for superlattice band structures approximating those of samples 4561, 4579 and 3756 in Fig. 8. The Landau miniband energy widths have been approximated with the function $\Delta_n(B)=\Delta_\alpha e^{-\alpha(n+1/2)\hbar\omega_c}$ where Δ_α and α are parameters obtained from fits to the results of $\mathbf{k}\cdot\mathbf{p}$ simulations. Both samples are simulated with $T=100$ K and electric field $F=F_c/2$ such that results are close to the Ohmic miniband transport regime but show some ballistic behavior.

The simulation results for low miniband widths [Figs. 8(a) and 8(b)] display two clear features: first, there is a pronounced minimum in the drift velocity (corresponding to a resistivity maximum) at the conventional MPR condition, and second, there are peaks in drift velocity at the SLMPR conditions. These results show excellent agreement with the schematic picture previously discussed. The simulations identify that the magnetotransport is dependent on both the scattering rate and the positions on the dispersion curves of the initial and final states. Resistance maxima at the MPR are caused by the increased scattering rate. The resistance minima at the SLMPR are formed from the relative effects of electric field acceleration in the initial and final scattering states.

Similar simulation results are observed for other samples which show that the position of the SLMPR feature is well described by Eq. (2), shifting progressively away from the LMPR feature with increasing miniband width. The simulation results change significantly when the miniband width becomes large $[\Delta_0(B)>\hbar\omega_{LO}]$ as observed for sample 3756 [Fig. 8(a)]. We observe that resistivity minima now occur at the $\delta n=1$ and $\delta n=1/2$ MPR conditions. This is in good

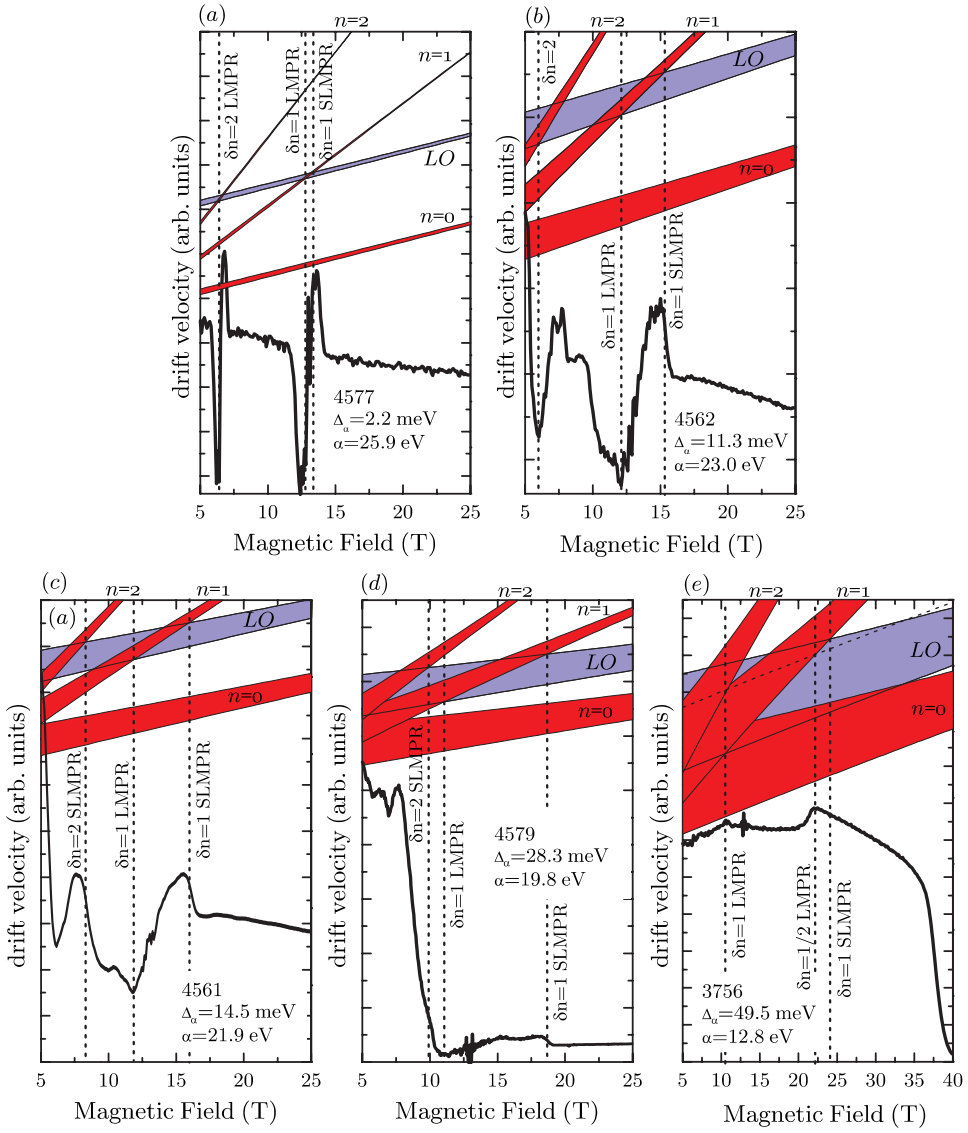

FIG. 8. (Color online) Monte Carlo simulation results for (a) sample 4577, $\Delta_\alpha=2.2$ meV, $\alpha=25.9$ eV^{-1}, (b) sample 4562, $\Delta_\alpha=11.3$ meV, $\alpha=23.0$ eV^{-1}, (c) sample 4561, $\Delta_\alpha=14.5$ meV, $\alpha=21.9$ eV^{-1}, (d) sample 4579, $\Delta_\alpha=28.3$ meV, $\alpha=19.8$ eV^{-1}, and (e) sample 3756, $\Delta_\alpha=48.5$ meV, $\alpha=12.8$ eV^{-1}. All are simulated for $T=100$ K and $F=F_c/2$. Shaded bands represent the approximated Landau level fan. Vertical dashed lines mark the SLMPR and MPR conditions. For sample 3756 a diagonal dashed line indicates the $n=0$ LLMB at $k_z=0$ plus $2\hbar\omega_{LO}$, marking the $\delta n=1/2$ MPR condition.

agreement with the bulk approximation in which the LMPR is observed as a resistivity minimum slightly below the MPR condition.[14] For sample 3756, the $\delta n=1/2$ MPR feature is particularly enhanced by proximity to the SLMPR condition. The SLMPR feature is, however, suppressed above the $\delta n=1/2$ MPR condition due to efficient intraminiband LO phonon emissions.

Our overall conclusion therefore is that the modeling provides strong support for the attribution of the high-field resistivity minimum to the predicted SLMPR feature, and that this is strongly supported by the clear dependence of the SLMPR position on miniband width.

By contrast, the attribution of a maximum or minimum in resistance to the precise MPR condition is not found to hold experimentally. The stronger feature is found to be a maximum at fields a few percent above the MPR condition. A resistivity minimum is found in all samples slightly below the MPR condition, in an analogous behavior to that seen in bulk material. The nonobservation of the SLMPR feature in the earlier GaAlAs-based work is probably due to the complications caused by the presence of the two phonon modes and the relatively small range of miniband widths studied.

In summary, we have demonstrated a form of magnetophonon resonance that occurs due to the scattering of carriers from the top of the ground state miniband to the bottom of the next LLMB. This resonance, known as superlattice MPR, was first predicted by Polyanovskii in 1983. The resonance condition corresponds to taking carriers from the top of the miniband dispersion where they will have a negative differential velocity and moving them to the bottom of the band where they can be "recycled" through the positive conduction regime.

ACKNOWLEDGMENTS

Part of this work has been supported by EuroMagNET under the EU Contract No. RII3-CT-2004-506239 of the Sixth Framework "Structuring the European Research Area, Research Infrastructures Action" and by the Brazilian agency CNPq under Contract No. 308116/2004-6.

*r.nicholas@physics.ox.ac.uk

[1] D. Fowler, A. Patané, A. Ignatov, L. Eaves, M. Henini, N. Mori, D. K. Maude, and R. Airey, Appl. Phys. Lett. **88**, 052111 (2006).
[2] A. Patané, N. Mori, D. Fowler, L. Eaves, M. Henini, D. K. Maude, C. Hamaguchi, and R. Airey, Phys. Rev. Lett. **93**, 146801 (2004).
[3] N. Mori, C. Hamaguchi, L. Eaves, and P. Main, VLSI Des. **13**, 45 (2001).
[4] A. B. Henriques, R. S. Deacon, and R. J. Nicholas, Braz. J. Phys. **32**, 605 (2004).
[5] R. S. Deacon, R. J. Nicholas, and P. A. Shields, Phys. Rev. B **74**, 121306(R) (2006).
[6] H. Noguchi, J. P. Leburton, and H. Sakaki, Phys. Rev. B **47**, 15593 (1993).
[7] H. Sakaki, Jpn. J. Appl. Phys., Part 1 **28**, 313 (1989).
[8] L. Esaki and R. Tsu, IBM J. Res. Dev. **14**, 61 (1970).
[9] R. Tsu and L. Esaki, J. Appl. Phys. **75**, 320 (1994).
[10] E. E. Mendez, F. Agulló-Rueda, and J. M. Hong, Phys. Rev. Lett. **60**, 2426 (1988).
[11] M. Kast, C. Pacher, G. Strasser, E. Gornik, and W. S. M. Werner, Phys. Rev. Lett. **89**, 136803 (2002).
[12] V. L. Gurevitch and Y. A. Firsov, JETP Lett. **13**, 137 (1977).
[13] R. A. Stradling and R. A. Wood, J. Phys. C **1**, 1711 (1968).
[14] P. G. Harper, J. W. Hodby, and R. A. Stradling, Rep. Prog. Phys. **36**, 1 (1973).
[15] R. J. Nicholas, Prog. Quantum Electron. **10**, 1 (1985).
[16] R. J. Nicholas, in *Landau Level Spectroscopy*, 1st ed., edited by G. Landwehr and E. Rashba (Elsevier, Amsterdam, 1991), Chap. 13, pp. 779–816.
[17] J. R. Barker, J. Phys. C **6**, 880 (1973).
[18] P. Kleinert and V. V. Bryksin, Phys. Rev. B **56**, 15827 (1997).
[19] W. M. Shu and X. L. Lei, Phys. Rev. B **50**, 17378 (1994).
[20] V. M. Polyanovskii, Sov. Phys. Semicond. **14**, 1411 (1980).
[21] V. M. Polyanovskii, Sov. Phys. Semicond. **17**, 1150 (1983).
[22] H. Noguchi, H. Sakaki, T. Takamasu, and N. Miura, Phys. Rev. B **45**, 12148 (1992).
[23] P. Gassot, J. Genoe, D. K. Maude, J. C. Portal, K. S. H. Dalton, D. M. Symons, R. J. Nicholas, F. Aristone, J. F. Palmier, and F. Laruelle, Phys. Rev. B **54**, 14540 (1996).
[24] K. S. H. Dalton, V. J. Hales, D. M. Symons, R. J. Nicholas, P. Gassot, D. K. Maude, and J. C. Portal, in *Proceedings of the 25th International Conference on the Physics of Semiconductors, parts I and II*, Springer Proceedings in Physics, Vol. 87 (Springer, Berlin, 2001), p. 907.
[25] V. J. Hales, A. J. Poulter, and R. J. Nicholas, Physica E (Amsterdam) **7**, 84 (2000).
[26] P. C. Klipstein, S. G. Lyapin, N. J. Mason, and P. J. Walker, J. Cryst. Growth **195**, 168 (1998).
[27] R. Deacon, R. Nicholas, A. Henriques, and N. Mason, Physica E (Amsterdam) **22**, 316 (2004).
[28] G. Bastard, Phys. Rev. B **24**, 5693 (1981).
[29] G. Bastard, Phys. Rev. B **25**, 7584 (1982).
[30] An example of results obtained using this method can be found at www-rjn.physics.ox.ac.uk/research/kptheory
[31] A. O. Govorov and M. V. Èntin, Solid State Commun. **92**, 977 (1994).
[32] V. V. Bryxin and Y. A. Firsov, Solid State Commun. **10**, 471 (1971).
[33] R. L. Peterson, in *Semiconductors and Semimetals*, edited by R. K. Willardson and A. C. Beer (Academic, New York, 1975), Vol. 10.